A new automated method for improving georeferencing of nighttime ECOSTRESS thermal imagery

Authors:

- Agnieszka Soszynska [1] (a.soszynska@utwente.nl)
- Harald van der Werff [1]
- Jan Hieronymus [2]
- Christoph Hecker [1]

1 Department of Applied Earth Sciences, Faculty ITC, University of Twente

2 Department of Computer Science, Humboldt-Universität zu Berlin

This paper has not been peer reviewed.

A new automated method for improving georeferencing of nighttime ECOSTRESS thermal imagery

Agnieszka Soszyńska[1], Harald van der Werff[1], Jan Hieronymus[2], and Christoph Hecker[1]

[1]Department of Applied Earth Sciences, Faculty ITC, University of Twente
[2]Department of Computer Science, Humboldt-Universität zu Berlin

November 2022

Abstract

Georeferencing accuracy plays a crucial role in providing high-quality ready-to-use remote sensing data. Georeferencing of satellite imagery is typically based on position and pointing direction of a sensor, which are provided by star trackers and GPS. As the Ecosystem Spaceborne Thermal Radiometer Experiment on Space Station (ECOSTRESS) is not equipped with star trackers, georeferencing of its imagery is based on the inaccurate knowledge about the location of its platform (the International Space Station) and later adjusted by image matching to the Landsat Orthobase. Although the georeferencing accuracy for daytime imagery is relatively high, we have observed that the nighttime imagery in Olkaria (Kenya), exhibits errors of 13.7 pixels on average, but in extreme cases even 62 pixels. Image based georeferencing in nighttime thermal satellite imagery is challenging, due to complexity of thermal radiation patterns in diurnal cycle and coarse resolution of thermal sensors in comparison to sensors imaging in the visual spectral range. Our paper introduces a novel approach for improved georeferencing of nighttime thermal imagery. We use object based matching of water bodies to an up-to-date landcover reference with high geolocation accuracy. Dynamically changing land cover often renders (static) land cover data bases unusable as a reliable reference basemap. We overcome this issue by automatically creating an up-to-date landcover reference to match acquisition time of the target image. Additionally, we use object based matching to account for lower spatial resolution of thermal sensors, as well as potential sharpness issues. In our method, edges of water bodies serve as matching objects, as they exhibit a relatively high contrast to adjacent areas. Results show that our method improves the existing georeferencing of ECOSTRESS images by 10.6 pixels on average, and an average accuracy of ± 3.1 pixels is achieved. The accuracy of our method depends on accurate cloud masks, because cloud edges can be mismatched as water-body edges and included in fitting of transformation parameters. We tested our method on ECOSTRESS imagery, but it is possible to be used with data from other sensors as well.

Keywords — remote sensing, automated georeferencing, image matching, thermal infrared, water bodies, changing land cover, Sentinel-2, ECOSTRESS

1 Introduction

Georeferencing accuracy is crucial for any remote sensing analysis. Satellite sensors equipped with star trackers in addition to GPS, allow a determination of location and pointing direction, which yields accurate georeferencing of a remotely sensed image. However, star trackers may malfunction, can be blinded by the sun, or might simply be lacking. For instance, the Ecosystem Spaceborne Thermal Radiometer Experiment (ECOSTRESS) mounted on the International Space Station (ISS), is not equipped with a star tracker. If its georeferencing were solely based on the position and attitude of the ISS, errors of approximately 2200 m would appear (which translates to an offset of approximately 31 pixels) [Smyth and Logan, 2020]. In such cases, image-based matching to reference basemap is often used to provide more accurate georeferencing.

Thermal Infrared (TIR) sensors currently operating in space typically have a coarser spatial resolution than visible reference imagery. In matching to a basemap, objects that are typically used as tie points, such as road crossings and edges of anthropogenic objects, are often not resolved in TIR imagery. Additionally the thermal infrared signature of objects can be vastly different from the signature in VIS-SWIR wavelengths, or even lack a

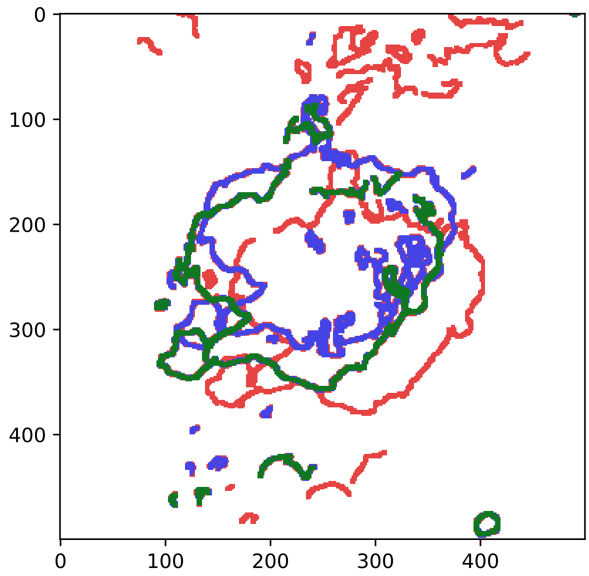

Figure 1: An example of georeferencing errors in nighttime ECOSTRESS images. The edges of water bodies (red, green, and blue) in 3 different images are overlaid. Due to georeferencing errors, the edges are offset against each other.

distinct edge or a common texture. Thus, using a basemap created from VIS-SWIR imagery for image matching of thermal imagery does not always yield accurate results. At the same time, creating a reference basemap based on TIR imagery is challenging due to the dynamic change of heat in diurnal cycles of surfaces. Heating up of objects depends dominantly on solar illumination and weather conditions preceding the time of acquisition. In case of nighttime imagery, spatial patterns observed during daytime depend strongly on physical properties of surfaces, such as the pace of cooling down. This property, also known as heat decay, is dependent on heat capacity and emissivity, and consequently varies for different materials [Kuenzer and Dech, 2013]. Generally, the later in the night, the more time a surface gets to cool down before being imaged, at different rates for different materials. Therefore, objects that are warmer than their surroundings after sunset can become colder than their surroundings before dawn. An additional practical difficulty can be caused by image quality. If anthropogenic objects of geometric shapes are not resolved in an image, matching tie points created from specific pixels (e.g., corners) becomes very difficult.

The difficulties regarding georeferencing of nighttime TIR imagery can be seen *e.g.*, in ECOSTRESS imagery. Standard processing of ECOSTRESS imagery involves image matching to the Landsat Orthobase [Smyth and Logan, 2020]. This reference basemap is created from data acquired in visual (VIS) up to short-wave infrared (SWIR) wavelength ranges, although ECOSTRESS images the TIR wavelength region in five spectral bands. The matching included in ECOSTRESS standard processing is based on 2-D fast Fourier transforms that create tie points between an image and the orthobase [Leprince et al., 2007]. The method works well in daytime imagery [Smyth and Logan, 2020] and especially in areas, where anthropogenic structures are numerous. Radiation during nighttime, however, tends to behave differently than during the day, which means that different spatial patterns are visible in the imagery. Our research shows that in areas, where infrastructure is scarce (like the region of the East African Rift), georeferencing of nighttime images of ECOSTRESS is not particularly accurate and errors of 62 pixels (4340 m) can be found, as shown in Figure 1. This is likely due to the lack of accurate tie points, which form the base for the georeferencing. A possible solution could be to use object based matching for georeferencing, where each match is based on testing the alignment of a larger visible object (*i.e.* many pixels at a time), instead of a single pixel match.

In areas where infrastructure is not strongly developed, matching needs to be based on natural structures, such as land cover classes. Land cover classes, however, exhibit complex radiation behaviour which results in differences in visibility of specific surfaces throughout diurnal cycle. There is, however, a land cover class which is easy to distinguish in nighttime thermal imagery: water bodies. Water bodies, in contrast to rocks and soil, maintain a relatively stable temperature over the course of a day due to the higher heat capacity and constant movement of particles [Engineering ToolBox, 2003]. Hence, their emitted radiation is relatively constant, compared to the diurnal amplitude of radiation of rocks and soils, and in consequence water bodies maintain high contrast to their surroundings. The overall high contrast of water bodies to their surroundings gives opportunities for image

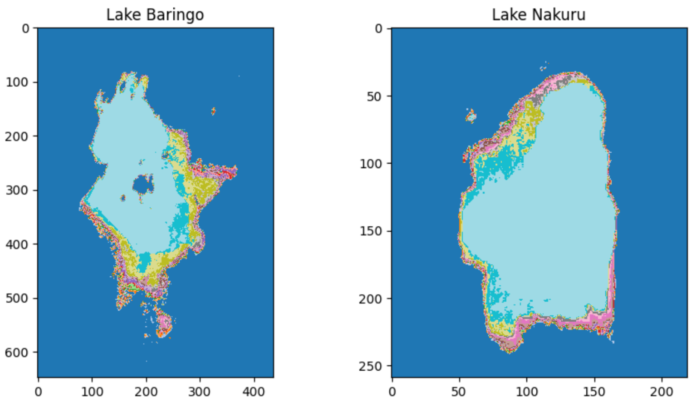

Figure 2: Changes in the spatial extent of water bodies due to varying water levels. This example shows two lakes in the East African Rift with dynamic water levels due to an increase in rainfall in the last 15 years [Government of Kenya & UNDP, 2021]. The different colours is the images represent different water levels between 2018 and 2022.

matching. Water bodies, however, are also of dynamic nature, as can be seen in Figure 2, which depicts the extent of two lakes in the East African Rift over the course of 4 years.

Oliver et al. [2022] showed that using static GIS data of water bodies is not reliable for sensitive mapping (such is georeferencing), because marked boundaries were consistently incorrect. This also applies to other water bodies data, such as *ASTER water body database* [NASA/METI/AIST/Japan Spacesystems and U.S./Japan ASTER Science Team, 2019]. It is, therefore, necessary to have an up-to-date, reference with high georeferencing accuracy for each to-be-georeferenced target image, if matching is based on water bodies. Such reference data should be acquired within short time window around the acquisition of target image (*e.g.*, one month), to maintain the highest possible similarity in water body extent. An example of a sensor capable of providing such reference data is Sentinel-2 MSI. With two sensors (S2A and S2B) currently operational, the Sentinel-2 mission has a repeat overpass of 5 days, which increases the probability of getting cloud-free data of a given area [Drusch et al., 2012]. The Sentinel-2 MSI instruments have 13 super-spectral bands of 10–60 m spatial resolution, covering VIS, Near InfraRed (NIR), and SWIR wavelengths with a 290 km swath width [Berger et al., 2012]. The absolute geolocation error of Sentinel-2 imagery is reported to be maximum 7.1 m for S2A and 4.6 m for S2B (at 95% confidence) (S2 MSI ESL team [2022]). Also the ground sampling distance (GSD) of Sentinel-2 MSI is higher than that of currently available TIR sensors (Table 1), which is advantageous for creating a reference for any sensor with similar parameters. The short revisit time, high spatial resolution, and georeferencing accuracy make this sensor an optimal choice for creating a regularly updated reference basemap by avoiding cloud cover and allowing worldwide coverage at a relatively high spatial resolution.

In this paper, we present a method for georeferencing of night-time thermal remote sensing images against a reference dataset of water bodies updated on a monthly basis. We test the method on ECOSTRESS imagery, and validate the achieved accuracy by analysing manually set checkpoints. In our georeferencing, we derive x-offset, y-offset, and rotation for each image. Generally, it is possible to also account for scaling and shearing; the number of parameters to-be-fitted is a function of number of valid tie points found. By manually assessing ECOSTRESS imagery, we did not find any images where transformation including scaling or shearing would be necessary, so we decided to opt for less transformation parameters and lower minimal number o tie points for the improvement process to take place.

2 Method

The processing chain for automated georeferencing of ECOSTRESS contains the following steps:

- Preparation of Sentinel-2 reference layer
- Preparation of ECOSTRESS image for matching
- Feature matching
- Filtering of matches
- Fitting transformation parameters

Table 1: The ground sampling distances of currently operational thermal sensors in comparison to the ground sampling distances of Sentinel-2 MSI.

Sensor	**GSD of thermal bands**
LANDSAT-8	100 m
LANDSAT-9	100 m
LANDSAT-7	60 m
VIIRS	750 m for M-bands, 375 m for I-bands
MODIS	1000 m
SLSTR	1000 m
ECOSTRESS	70 m
ASTER	70 m
Sensor	**GSD**
Sentinel-2 MSI	10 m, 20 m, 60 m

- Resampling of the original ECOSTRESS image

2.1 Preparation of the reference layer

The first step is to prepare a reference layer for georeferencing improvement of ECOSTRESS.

The Google Earth Engine [GEE, Gorelick et al., 2017] is used to collect and process Sentinel-2 MSI data acquired from January 2018 onwards. The "Scene Classification Layer" (SCL) that comes with the level-2 product is a land cover map with the following classes: No data, saturated defective pixels, topographic cast shadows, cloud shadows, vegetation, non-vegetated areas, water, unclassified, cloud medium probability, cloud high probability, thin cirrus, and snow or ice [ESA, n.d.]. For the purpose of generating a monthly reference image of water bodies, the SCL is aggregated per calendar month, resulting in 12 products for each year, 48 products for the years 2018–2022. The water class is of highest importance, but we also use shadow, snow, and cloud classes to correct the reference layer for missing information when water would be invisible. Pixels labeled as "clouds", "cloud shadow" or "snow" are masked by assigning a value of 0 (zero, meaning "no data"). Pixels labeled as "dark pixels", "bare soil", "vegetation" or "water" are kept at their original values (2, 4, 5, and 6, respectively). The so-called "quality-mosaic" functionality in GEE, in which scenes are aggregated in an order of highest pixel value to lowest, is used to label pixels from highest to lowest values found in each pixel for each calendar month. This implies that, for each pixel, the label "water" (with a value of 6) precedes over labels vegetation, bare soil, dark pixels, and masked pixels; in that order. The resulting aggregate will therefore contain the maximum water extend within each calendar month.

For georeferencing of a target image, the water mask of the respective acquisition month is chosen. The water mask is reprojected from the original spatial resolution of 20 m to match the projection of ECOSTRESS data at 70 m . In the reprojected water masks, each water body is automatically labelled. The derived labels later allow identifying the edges of a specific water body in the reference image. We restricted the minimal water body size to at least 50 pixels, so that it yields sufficient edge pixels for comparison. To create the actual reference layer, Canny edge gradient operator is then applied to the labelled image so that water body edges are derived. The edges are subsequently dilated by ± 1 pixel horizontally and vertically, to find the correct position of the water body in target image more efficiently. If the water body extent in reference and target images would differ by even 1 pixel, the matching process would fail more frequently, by *e.g.*, matching only a part of a water body edge, and subsequently not fulfill the validity criteria (which are described later); this is avoided by dilation of edges. As a final step, the Sentinel-2 reference is cloud-masked using both the Sentinel-2 cloud mask and cloud mask from the target image.

2.2 Preparation of the ECOSTRESS images

The main purpose of ECOSTRESS mission is to provide several atmospherically corrected higher-level products for vegetation stress analysis, such as a land surface temperature and emissivity product (LSTE) and an evapotranspiration product (ET). Several metadata come with these image files, which include quality flags per pixel as indicator for cloud detection and land surface temperature accuracy.

A set of 27 ECOSTRESS images with varying cloud cover was used to test our georeferencing method (see Appendix A). These images are first automatically georeferenced using the L1B-GEO files provided with the LSTE files. A georeferencing python script is provided in the package Pyresample [Hoese and Lahtinen, 2021], which is a part of the standard processing of images in APPEEARS service [NASA JPL, n.d.]. In our processing,

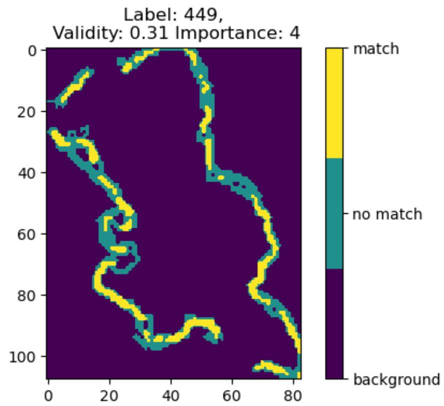

Figure 3: An example of a matched water body. Some pixels can be missing due to cloud cover or image quality.

we used a georeferencing script with the same principle, adapted to provide annotations for quality flags per pixel in addition to the image product.

Each image is then cloud masked using the "quality flags" metadata provided with the imagery. Cloud masks can contain errors, which have significant impact on accuracy of matching, therefore to account for mistakes in the cloud mask, statistics-based thresholding method is used to mask clouds as well. The threshold is derived by fitting a Gausssian function on the LST histogram; all pixels with values below mean minus 1.5 standard deviation ($\mu - 1.5\sigma$) are treated as clouds and masked in the image. The cloud mask and bounding box edges are dilated by 9 × 9 pixels, to avoid confusion with the edges of clouds that could lead to inaccurate matches.

Next, the masked images are normalised so that the values fit between 0 and 255, which is required for the Canny edge operator in the OpenCV library [OpenCV, n.d.]. To account for radiometric errors and very cold clouds, the normalization minimum and maximum is set to 1^{st} and 99^{th} percentile. The Canny edge gradient operator is applied to obtain a binary image that contains only edges, which are dilated in the same manner as the reference image, to make the matching process more efficient by compensating for 1-pixel water body extent differences between reference and target . Due to the high contrast between water bodies and surrounding land in nighttime TIR imagery, the water body edges are the strongest in the gradient image. As a final step, the cloud masks (including the cloud mask from reference image) are applied to the target images.

2.3 Match edges of water bodies between target and reference images

In our method, we use object (*i.e.*, water body) matching procedure based on a brute force principle to compare overlap of the edges of water bodies in the target and reference images within a search window.

This process starts with identifying the edges of each labelled water body in the reference layer. For each labelled water body, a search window in the target image extending ±75 pixels from the reference water body location is extracted. This relatively large search window accounts for a georeferencing error of similar size. To automatically locate a given water body in the target image, a target image fragment, which can potentially contain the water body is compared to the reference. The position of the target image fragment is iteratively shifted over the search window, one pixel in x- and y-direction at a time, and a comparison of overlap between the reference and target is repeated for each position. The overlap in each position is verified by adding the binary edges in the reference and target fragments. The accuracy is expressed by a histogram of image values: 0 (background), 1 (not matching edges), and 2 (matching edges) (Figure 3). The optimal position is subsequently given by the highest number of matching edges and saved as "tie point" for finding the transformation matrix parameters later on.

2.4 Filtering tie points and fit transformation parameters

After the iteration through all the water bodies in an image, a set of tie points is obtained. Some of these tie points can be incorrect (for instance due to edges of cloud remnants and features on the Earth surface) and they need to be filtered out. Several selection criteria are defined to filter the pixels used for matching and to filter the resulting transformation parameters.

The criteria "validity" and "importance" are defined for filtering tie points: Validity is given by fraction of water body pixels in the reference image that are matched in the target image (Figure 3). Importance is a custom parameter that reflects for each image fragment the size of a water body and the distribution of matching pixels:

size of a water body in pixels If the number of matching pixels exceeds 60, importance is raised by 1. If the number of matching pixels exceeds 200, importance is again raised by 1.

distribution of matching pixels If matching pixels are located in two or three quadrants, importance is raised by 1. If matching pixels are in all quadrants, importance is raised by 2.

After filtering the bad matches by the parameters "validity" and "importance", additional step is to sieve out tie points that produce outlying transformation parameters. All combinations of two tie points are used to define transformation parameters and, with each obtained set of transformation parameters, all tie points are subsequently transformed. The Euclidean distance between tie point location in the original ECOSTRESS image and the transformed image is calculated, and points exceeding 3 pixels are treated as outliers. Filtering those outliers allows to determine the optimal set of parameters.

After removing incorrect tie points, final transformation parameters for georeferencing are determined if two or more valid matches remained, which allows fitting of x- and y-offset, and rotation. A nearest-neighbour resampling is used to apply the transformation parameters to an ECOSTRESS image.

2.5 Validation

After the resampling, meta data for each image is generated, which includes Euclidean distances between tie points in the transformed target coordinates and coordinates from the reference layer. These distances provide an absolute error for each point and further mean absolute error for each dataset, and thus serve as an information on residual error and accuracy measure of the transformation. Additionally, this gives also information on reliability of the transformation provided by number of tie points used - the more tie points, the more reliable the fitted parameters are, especially if the final Euclidean distances are low.

To test the accuracy of our method, we compared the transformed target image to the reference base map and manually set ground control points (check points) in both images based on user photo-interpretation. For each image, the parameter "mean", "median", "standard deviation" and "change" was saved. A set of check points was defined evenly distributed over each entire image, so that errors related to rotation are retrieved. The standard deviation provides information on larger errors that could be found at image edges due to extrapolation. Parameter "change" is calculated by subtracting the mean error per image in not transformed images from their transformed counterparts: The higher the value, the bigger the improvement in geolocation by our method. Negative values indicate that the error in the original image was lower.

3 Results

The boxplots in figure 4 show the difference between the georeferencing provided by the data supplier in Build 6 and the results of our method ("This work"). Out of the 27 images used in this test, 24 could be processed. The remaining 3 could not be processed, because the ECOSTRESS cloud masks covered all the water bodies (although the water bodies were visible in the LSTE images). The fitted transformation parameters can be seen in Table 2. Most of the transformation bases on x- and y-offsets; while rotation fitted for each image does not exceed 0.1°. Table 3 shows the mean Euclidean distance between the reference and transformed tie points, which ranges between 0.1 and 1.9 pixels, The average error is 1.3 pixels.

The second validation, based on check points, is presented in Table 4. These results show a considerable spread in the fit of check points. This seems to happen when tie points used to define the transformation matrix are located in only one part of the image: Errors appear in areas distant from the tie points, especially when an image is rotated. Figure 5 illustrates how such an error propagates over an image.

4 Discussion

High accuracy of georeferencing is a crucial requirement for any remote sensing analysis. In case of thermal space-borne imagery, matching algorithms typically used for image-based georeferencing often do not work, because of dynamic diurnal changes of surface temperature. Especially if man-made structures (such as highways or road crossings) are not well visible, few tie points can be found to support the matching process. We have observed that ECOSTRESS images appear less sharp than, for instance, ASTER images which means that man-made structures are often not resolved enough to provide a tie point. Therefore, matching whole objects, such as water bodies, instead of specific pixels can yield much better results. We propose a novel approach to georeferencing improvement, specially designed for thermal IR nighttime imagery.

In our approach, we use matching based on edges of water bodies, which are well visible in thermal images. We create a reference dataset for each calendar month, which accounts for seasonal as well as long-term changes of water level.

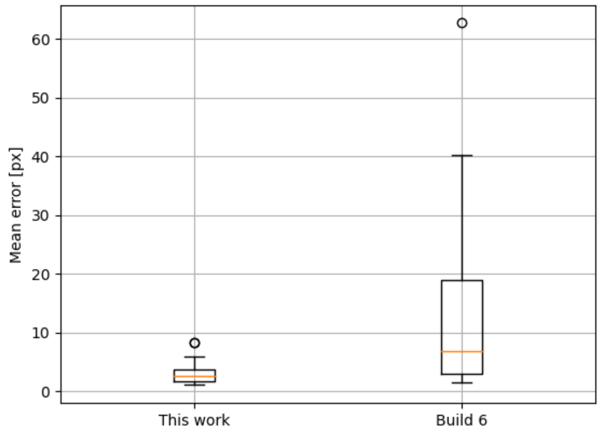

Figure 4: Mean georeferencing error in images improved with our method ("This work") and with standard ECOSTRESS processing only ("Build 6").

Table 2: Fitted transformation parameters

Dataset	**X-offset [px]**	**Y-offset [px]**	**Rotation [°]**
20190803T210453	10	-1	-0.03
20191022T013248	4	5	-0.02
20200109T180437	4	7	0.00
20200518T025952	0	1	-0.02
20200602T204208	10	2	-0.04
20200827T223216	9	-25	-0.05
20200831T205833	10	4	0.03
20200924T000312	1	-6	0.07
20201001T205854	9	8	-0.09
20201005T192641	9	-13	0.16
20210204T190212	2	-4	0.05
20210312T050515	0	-1.3	0.03
20210324T002716	1	-3	-0.03
20210717T025340	-10	50	-0.34
20210724T234916	5	48	-0.20
20210818T020947	7	-15	0.01
20210923T000600	20	-14	-0.01
20211017T022738	15	7	0.03
20211118T014738	21	-22	-0.01
20211207T180801	44	-40	-0.20
20211227T215613	2	0	-0.01
20220306T184938	1	-5	-0.02
20220314T040423	2	1	-0.01
20220322T005432	1	-3	0.02

Table 3: Euclidean distance between reference and transformed tie points.

Image	Mean [px]	Tie points Euclidean distance [px]							
20190803T210453	1.0	0.6	1.1	0.4	0.8	1.4	1.2	1.2	
20191022T013248	0.4	0.3	0.8	0.5	0.2				
20200109T180437	1.8	2.0	0.8	1.8	2.5	2.1			
20200518T025952	1.1	1.0	0.4	2.0	1.4	0.5	1.3	1.0	
20200602T204208	0.1	0.1	0.1						
20200827T223216	1.8	1.7	1.2	2.7					
20200831T205833	1.0	0.8	1.1	1.2	1.9	0.3	0.8		
20200924T000312	1.3	1.6	0.7	0.5	1.6	1.4	1.9	1.1	
20201001T205854	1.8	0.9	1.5	2.6	2.3				
20201005T192641	1.7	2.0	1.3	1.6					
20210204T190212	1.6	2.6	1.3	0.9	1.1	1.1	1.8	1.2	2.8
20210312T050515	1.2	1.2	1.2	0.3	2.6	1.1	0.8		
20210324T002716	1.4	1.3	2.1	0.4	0.3	2.8	1.3	1.0	1.9
20210717T025340	1.8	1.8	1.8						
20210724T234916	0.5	0.7	0.6	0.3					
20210818T020947	1.4	1.1	0.8	1.6	2.0	1.3			
20210923T000600	1.9	1.1	2.0	2.0	1.6	2.7			
20211017T022738	1.2	0.6	0.5	1.8	0.7	2.1			
20211118T014738	1.3	2.1	0.6	1.7	1.0				
20211207T180801	1.6	1.8	2.2	0.3	2.1				
20211227T215613	1.7	0.8	1.6	2.4	2.1	1.5	1.7		
20220306T184938	1.4	0.9	1.3	2.5	0.8	1.5			
20220314T040423	1.4	1.9	0.6	0.8	0.8	2.6	2.5	1.3	1.9
		0.9	0.8	0.3	0.9	1.2	2.0	0.8	
20220322T005432	1.1	1.0	1.4	1.7	0.8	1.4	0.3	1.3	

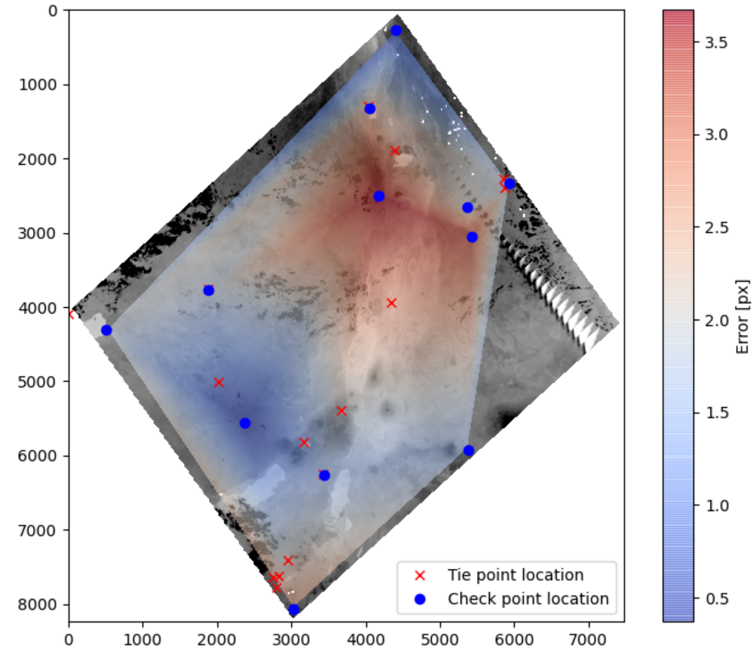

Figure 5: An example error interpolation plotted on background of the original target image. The area where no tie points are located exhibits the highest errors. It is possible that check points are also set with an offset, due to user error, and/or sharpness of the image. The error interpolation plot reaches only the most external check point, which is why the shape of the image and error plot are not matching.

Table 4: Error derived from manual check point setting.

Image	**Check point Euclidean distance [px]**										
20190803T210453	3.5	7.1	0.7	0.6	2.5	0.4	1.0	4.4	8.7	8.2	2.8
20191022T013248	1.3	1.0	1.5	4.2	1.2	1.8	2.6	2.2			
20200109T180437	0.4	2.8	2.0	4.6	3.6	2.4	1.6				
20200518T025952	0.6	0.7	4.0	0.8	0.9	1.0	1.0	2.6			
20200602T204208	3.6	2.2	2.5	1.0	3.0	2.4	4.4	2.4			
20200827T223216	2.0	2.5	2.4	4.9	2.0	3.3	2.0	1.6			
20200831T205833	0.7	1.1	0.9	0.9	2.3	1.8	0.2	3.0	3.3	2.0	
20200924T000312	1.0	3.6	4.9	3.2	7.0	1.0	2.9	1.7			
20201001T205854	1.4	8.3	4.5	2.9	2.1	1.9	8.7	1.5			
20201005T192641	6.5	6.1	11.4	2.3	0.9	1.7	1.1				
20210204T190212	2.0	1.0	2.7	1.0	1.4	1.3	3.8	0.8			
20210312T050515	6.4	7.6	11.4	8.6	12.3	7.8	6.3				
20210324T002716	1.3	2.6	1.1	2.2	1.6	2.3	1.2	0.9	1.6	2.2	2.1
20210717T025340	19.0	2.0	5.1	6.5	3.1	11.1	10.9				
20210724T234916	6.4	4.0	0.5	3.3	9.2	7.3	11.0				
20210818T020947	2.8	6.5	4.5	4.4	4.5	5.2	1.2	2.3	1.4	1.7	3.0
20210923T000600	2.1	2.3	0.7	2.0	2.2						
20211017T022738	7.2	1.5	1.1	5.0	1.9	3.8	2.2	4.1			
20211118T014738	0.8	1.3	0.7	0.3	1.4	1.5					
20211207T180801	2.0	2.5	7.5	2.5	6.3	4.2					
20211227T215613	0.8	1.5	2.6	0.8	1.8	1.3					
20220306T184938	1.3	0.8	1.5	0.7	1.2	1.5	2.6	3.1	1.4	5.0	
20220314T040423	0.9	1.0	2.8	1.2	1.3	1.8					
20220322T005432	2.5	1.5	0.2	1.3	0.7	1.2	0.2				

Table 5: Statistical measures of error for each image.

Image	**Mean [px]**	**Median [px]**	**Stdev [px]**	**Change [px]**
20190803T210453	3.6	2.8	2.9	5.4
20191022T013248	2.0	1.6	1.0	3.3
20200109T180437	2.5	2.4	1.3	4.6
20200518T025952	1.4	0.9	1.1	1.1
20200602T204208	2.7	2.5	0.9	3.0
20200827T223216	2.6	2.2	1.0	26.9
20200831T205833	1.6	1.4	1.0	11.5
20200924T000312	3.1	3.0	1.9	1.7
20201001T205854	3.9	2.5	2.8	-1.5
20201005T192641	4.3	2.3	3.6	-1.8
20210204T190212	1.7	1.3	1.0	-0.2
20210312T050515	8.6	7.8	2.2	-7.0
20210324T002716	1.7	1.6	0.5	2.7
20210717T025340	8.2	6.5	5.5	-3.1
20210724T234916	5.9	6.4	3.4	11.8
20210818T020947	3.4	3.0	1.6	27.8
20210923T000600	1.9	2.1	0.6	23.1
20211017T022738	3.3	3.0	2.0	16.7
20211118T014738	1.0	1.1	0.4	30.7
20211207T180801	4.2	3.4	2.1	58.5
20211227T215613	1.5	1.4	0.6	0.4
20220306T184938	1.9	1.4	1.3	4.9
20220314T040423	1.5	1.2	0.6	1.1
20220322T005432	1.1	1.2	0.7	2.4

Our method improves the georeferencing of ECOSTRESS images by 10 pixels on average, and an average accuracy of ± 3.1 pixels is achieved. While perhaps the accuracy could be further enhanced, it is important to note that validation using manually set check point can also be faulty, because of relatively high edge spread. Our validation with manual check points (provided in Table 4 and Table 5) should be treated with caution; errors of ± 2 pixels in the validation are possible. If a check point located alone in one part of the image was set with an error, the analysis of transformation (as presented in Figure 5) could falsely suggest a rotation error. The tie point residuals (presented in Table 3) complement the information provided by manual check point setting and these fit parameters have an average accuracy of ± 1.2 pixels. Since the residuals are provided as meta data for each processed image, they can be used by all users for preliminary assessment of the transformation accuracy and reliability. If Euclidean distances are similarly low for all tie points, the georeferencing is likely to be accurate, whereas outliers suggest a larger error. High number of tie points increases the reliability of the georeferencing.

The accuracy of our method is supported by the values in column "Change" in Table 5. There are only few negative values in column "Change" and their absolute values are significantly smaller than average errors from the standard processing (13.7 pixels in nighttime imagery, Figure 4). This means that an error introduced by our processing is much smaller than the errors that are corrected. On average, our georeferencing algorithm decreases the georeferencing error from 13.7 pixels by 10.6 pixels to 3.1 pixels.

Our method depends on the visibility of objects on the Earth surface that can be matched. The largest obstacle in processing is cloud cover and imprecise cloud masking in both ECOSTRESS and in the reference data. If clouds are not masked properly, their edges will be treated as water body edges and used in feature matching, thereby introducing an error. We added filtering of tie points to remove such cases, but some errors remain nevertheless.

Additionally, some errors can appear due to georeferencing error of cloud masks, because cloud masks of both target and reference are used on both datasets. Thus, if a cloud covers an image in target image, but the georeferencing of this masks has an offset, the matching may be faulty. Such errors are possible despite filtering of tie points, however we did not observe such cases in the images we processed.

Our matching algorithm uses a brute force principle, by matching image fragments and shifting these fragment pixel by pixel. This means that our method does not consider rotation for each water body separately, and the geometric resolution of a tie point is limited to a pixel. However, the rotation error in ECOSTRESS imagery is very low (Table 2), so ignoring this does not influence accuracy strongly. In future, adaptions could be made, including matching water bodies with sub-pixel accuracy, and rotating each individual water-body. Possibly, algorithms, such as Iterative Closest Point could enhance the efficiency of matching.

It is important to note that our method considers the most up-to-date reference image but does not accommodate rapid weather or man-made events that change the contours of water bodies. If there is a dynamic change in the water level, temporal resolution of one month may not be enough. This can be adapted by reducing the time window around the acquisition of the target image, or even limiting reference data to the datasets between weather events, such as rainfall.

The reliability of the proposed georeferencing method strongly depends on the number of matches found during the process, as well as the quality of fit. It appears that images with the highest error values were processed with only a few tie points (Table 3). Generally, the more tie points used for fitting the transformation parameters, the more reliable it gets. In the area, where multiple key-points were found, the accuracy of georeferencing is very high, as can be seen in Figure 5. However, if tie points are concentrated in one part of the image, the accuracy of georeferencing in such image will not be homogeneous, especially if rotation is found. This is visible when analysing specific images with high standard deviation of errors (Table 5). The errors become higher in areas, where few water bodies are visible (*e.g.*, see errors for image 20210717T025340 in Table 4, which was processed using only 2 tie points (Table 3)).

Filtering the tie points is a very important step, which should sieve out wrong matches. Using only the larger water bodies avoided confusion between many small water bodies of similar shape. Wrong matches can have very strong influence on finding transformation parameters, which can result in a larger overall error. For instance, in image 20201005T192641, one wrong tie point was not filtered out, which influenced the whole transformation matrix; the average error for this image is 4.3 pixels.

Our filtering parameters are empirically derived, and possibly need adaption for other study areas. The larger the water body is and the more complex shape it has, the more reliable match it can provide. In future, filtering parameters could be defined, for instance, as a proportion of search window.

There is a trade-off between the harshness of filtering and the number of images that will not be processed at all due to insufficient remaining tie points. The user needs to decide upon the harshness of filtering, considering the application. Most efficiently, harshness of filtering can be changed by the parameter "importance" (*e.g.*, by using tie points with importance 4 only, to use only the most reliable tie points).

Errors can also appear due to other reasons. The reference images are acquired in different wavelengths than the target images. Differences may appear especially in areas, where land cover is more complex than classes provided in SCL, such as vegetation floating on water. In SCL, such areas will be classified as vegetation, but in

ECOSTRESS images they are seen as warmer than land surfaces, and in processing they are treated as water. Additionally, assumptions are made to create the classification layer, these assumptions may lead to differences in delimitation of a water body.

Lastly, misclassification errors in SCL layer additionally add to overall error per image. For instance, cloud shadows may contribute to misclassification in the SCL layer. The risk of maintaining an error in the reference image, however, is minimized due to the fact that for each month of acquisitions, a separate reference layer is created.

Generally, our method outperforms the current georeferencing of ECOSTRESS data and can be used globally provided that some water bodies (including shore lines) are present. Since ECOSTRESS scenes have a 384 km swath width), chances are that at least some water bodies should be present in an image.

With increasing availability of computational power, it is possible to focus on better image matching approaches to object based matching. Our research proves that using up-to-date reference yields accurate results. Since preparation of a large mosaic for referencing only takes few seconds in a cloud-based environment such as GEE, it is possible to use the most recent images from high resolution operational satellites with high georeferencing accuracy as a reference, instead of large reference data bases such as LANDSAT orthobase. In our processing, we downloaded the reference masks from GEE and run the process locally (which takes approximately 25 minutes per image), but if the approach were reversed and target images were uploaded to a cloud computing platform, the overall processing time might be strongly reduced.

5 Conclusions

High georeferencing accuracy is necessary for a reliable use of remote sensing data. We propose a novel approach to image-based georeferencing improvement for thermal IR data, specifically nighttime data. Our results show that matching nighttime thermal IR images to an up-to-date land/water mask leads to successful automatic tie point creation between image and reference. The results are reliable and robust as long as a number of water bodies are contained in the scene. In the case of ECOSTRESS night time images, our method resulted in a georeferenced product with a mean error of 3.1 pixels, compared to 13.7 pixels error in the original data. With a shift towards cloud computing, it is possible to both create a reference for each image and conduct the entire processing on the fly in the cloud.

References

M. Berger, J. Moreno, J. A. Johannessen, P. F. Levelt, and R. F. Hanssen. ESA's sentinel missions in support of Earth system science. *Remote Sensing of Environment*, 120:84–90, 2012. doi: 10.1016/j.rse.2011.07.023.

M. Drusch, U. Del Bello, S. Carlier, O. Colin, V. Fernandez, F. Gascon, B. Hoersch, C. Isola, P. Laberinti, P. Martimort, A. Meygret, F. Spoto, O. Sy, F. Marchese, and P. Bargellini. Sentinel-2: ESA's optical high-resolution mission for GMES operational services. *Remote Sensing of Environment*, 120:25–36, 2012. doi: 10.1016/j.rse.2011.11.026.

Engineering ToolBox. Water — Thermophysical properties, 2003. URL https://www.engineeringtoolbox.com/water-thermal-properties-d_162.html.

ESA. Sentinel-2 MSI level-2a algorithm overview. https://sentinel.esa.int/web/sentinel/technical-guides/sentinel-2-msi/level-2a/algorithm, n.d. Accessed November 2022.

N. Gorelick, M. Hancher, M. Dixon, S. Ilyushchenko, D. Thau, and R. Moore. Google Earth Engine: Planetary-scale geospatial analysis for everyone. *Remote Sensing of Environment*, 202:18–27, 2017. doi: 10.1016/j.rse.2017.06.031.

Government of Kenya & UNDP. Rising water levels in Kenya's rift valley lakes, Turkwel Gorge dam and Lake Victoria, 2021.

D. Hoese and P. Lahtinen. Pyresample, 2021. URL https://github.com/pytroll/pyresample/blob/main/docs/source/index.rst. Accessed November 2022.

C. Kuenzer and S. Dech. *Theoretical Background of Thermal Infrared Remote Sensing*, pages 1–26. Springer Netherlands, Dordrecht, 2013. ISBN 978-94-007-6639-6. doi: 10.1007/978-94-007-6639-6_1. URL https://doi.org/10.1007/978-94-007-6639-6_1.

S. Leprince, S. Barbot, F. Ayoub, and J.-P. Avouac. Automatic and precise orthorectification, coregistration, and subpixel correlation of satellite images, application to ground deformation measurements. *IEEE Transactions on Geoscience and Remote Sensing*, 45(6):1529–1558, 2007.

NASA JPL. Appeears, n.d. URL https://appeears.earthdatacloud.nasa.gov/. Accessed November 2022.

NASA/METI/AIST/Japan Spacesystems and U.S./Japan ASTER Science Team. Aster global water bodies database v001, 2019. URL https://doi.org/10.5067/ASTER/ASTWBD.001.

J. A. Oliver, F. C. Pivot, Q. Tan, A. S. Cantin, M. J. Wooster, and J. M. Johnston. A machine learning approach to waterbody segmentation in thermal infrared imagery in support of tactical wildfire mapping. *Remote Sensing*, 14(9):2262, 2022.

OpenCV. Canny edge, n.d. URL https://docs.opencv.org/3.4/dd/d1a/group__imgproc__feature.html#ga04723e007ed888ddf11d9ba04e2232de. Accessed November 2022.

S2 MSI ESL team. Data quality report Sentinel-2 l1c msi, July 2022, 2022. URL https://sentinel.esa.int/documents/247904/4766914/OMPC.CS.DQR.001.06-2022+-+i77r0+-+MSI+L1C+DQR+July+2022.pdf.

M. Smyth and T. L. Logan. ECOSTRESS science meeting L1B geolocation review, 2020.

A List of image identifiers

File ID	Paper ID
ECOSTRESS_L2_LSTE_06108_017_20190803T210453_0601_02	20190803T210453
ECOSTRESS_L2_LSTE_07336_021_20191022T013248_0601_02	20191022T013248
ECOSTRESS_L2_LSTE_08572_020_20200109T180437_0601_01	20200109T180437
ECOSTRESS_L2_LSTE_10578_018_20200518T025952_0601_01	20200518T025952
ECOSTRESS_L2_LSTE_10822_017_20200602T204208_0601_01	20200602T204208
ECOSTRESS_L2_LSTE_12156_025_20200827T223216_0601_01	20200827T223216
ECOSTRESS_L2_LSTE_12217_021_20200831T205833_0601_01	20200831T205833
ECOSTRESS_L2_LSTE_12576_007_20200924T000312_0601_01	20200924T000312
ECOSTRESS_L2_LSTE_12698_016_20201001T205854_0601_01	20201001T205854
ECOSTRESS_L2_LSTE_12759_016_20201005T192641_0601_01	20201005T192641
ECOSTRESS_L2_LSTE_14650_016_20210204T190212_0601_01	20210204T190212
ECOSTRESS_L2_LSTE_15199_015_20210312T050515_0601_01	20210312T050515
ECOSTRESS_L2_LSTE_15383_015_20210324T002716_0601_01	20210324T002716
ECOSTRESS_L2_LSTE_16001_021_20210502T203637_0601_01	20210502T203637
ECOSTRESS_L2_LSTE_17172_016_20210717T025340_0601_01	20210717T025340
ECOSTRESS_L2_LSTE_17294_018_20210724T234916_0601_01	20210724T234916
ECOSTRESS_L2_LSTE_17670_030_20210818T020947_0601_01	20210818T020947
ECOSTRESS_L2_LSTE_18228_017_20210923T000600_0601_01	20210923T000600
ECOSTRESS_L2_LSTE_18602_028_20211017T022738_0601_01	20211017T022738
ECOSTRESS_L2_LSTE_19099_015_20211118T014738_0601_01	20211118T014738
ECOSTRESS_L2_LSTE_19404_017_20211207T180801_0601_01	20211207T180801
ECOSTRESS_L2_LSTE_19716_033_20211227T215613_0601_01	20211227T215613
ECOSTRESS_L2_LSTE_20784_022_20220306T184938_0601_01	20220306T184938
ECOSTRESS_L2_LSTE_20899_011_20220314T040423_0601_01	20220314T040423
ECOSTRESS_L2_LSTE_21021_016_20220322T005432_0601_01	20220322T005432